Electronic Supplementary Material (ESI) for Inorganic Chemistry Frontiers.

SUPPORTING INFORMATION

Symmetry-Breaking Phase Transitions, Dielectric and Magnetic properties of Pyrrolidinium-Tetrahalidocobaltates

Martyna Ksiądzyna[a], Vasyl Kinzhybalo[b], Alina Bieńko[a], Wojciech Medycki[c], Ryszard Jakubas[a], Cyril Rajnák[d], Roman Boča[d], Andrew Ozarowski[e], Mykhaylo Ozerov[e], Anna Piecha-Bisiorek[a]*

[a] *Faculty of Chemistry, University of Wrocław, F. Joliot-Curie 14, 50-383 Wrocław, Poland*
[b] *Institute of Low Temperature and Structure Research Polish Academy of Sciences, Okólna 2, 50-422 Wrocław, Poland*
[c] *Institute of Molecular Physics, Polish Academy of Sciences, M. Smoluchowskiego 17, 60-179 Poznań, Poland*
[d] *Department of Chemistry, Faculty of Natural Sciences, University of SS Cyril and Methodius, 91701 Trnava, Slovakia*
[e] *National High Magnetic Field Laboratory, Florida State University, 1800 East Paul Dirac Drive, Tallahassee, Florida 32310,United States*

1. Experimental

Table S1. Element analysis of C, H and N for **PCC** and **PCB**.

Elements	C (%)	H (%)	N (%)
Calculation for **PCC**	27.85	5.84	8.12
Found for **PCC**	28.74	5.98	8.50
Calculation for **PCB**	18.38	3.86	5.36
Found for **PCB**	18.75	3.86	5.47

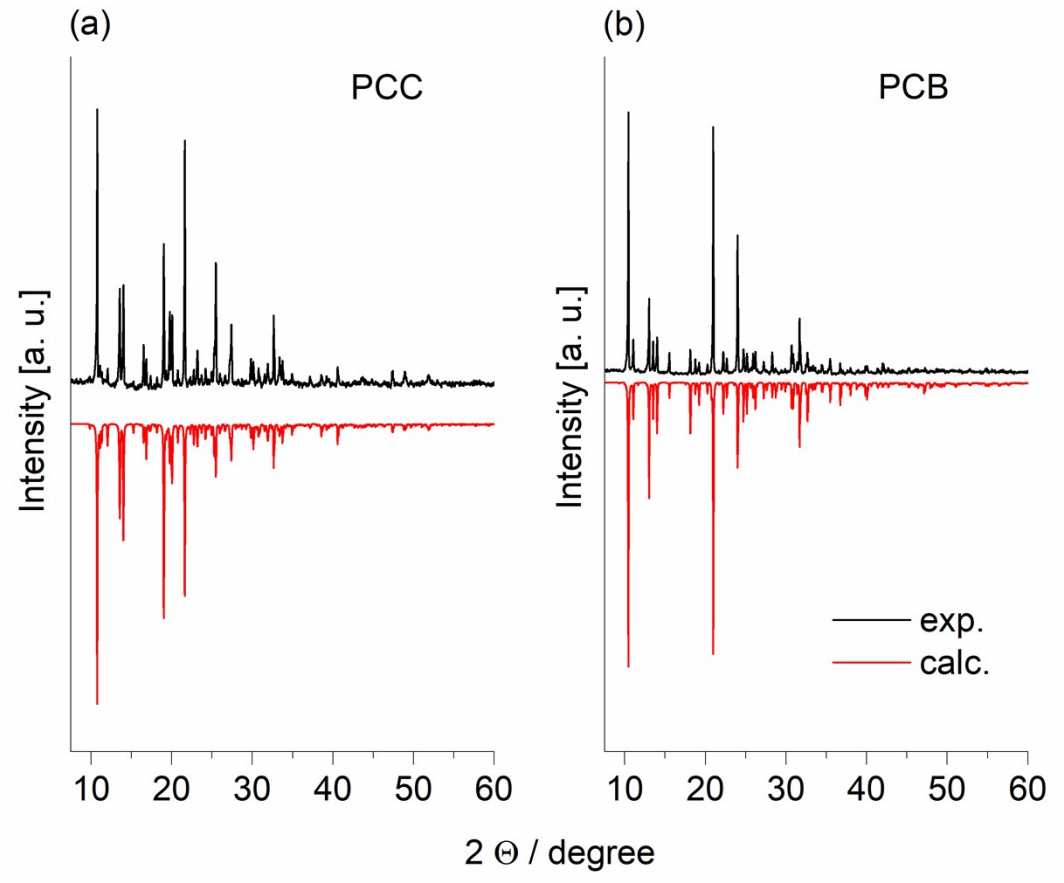

Figure S1. X-ray diffraction pattern at 298 K of (a) **PCC**; (b) **PCB**.

2. Thermal properties

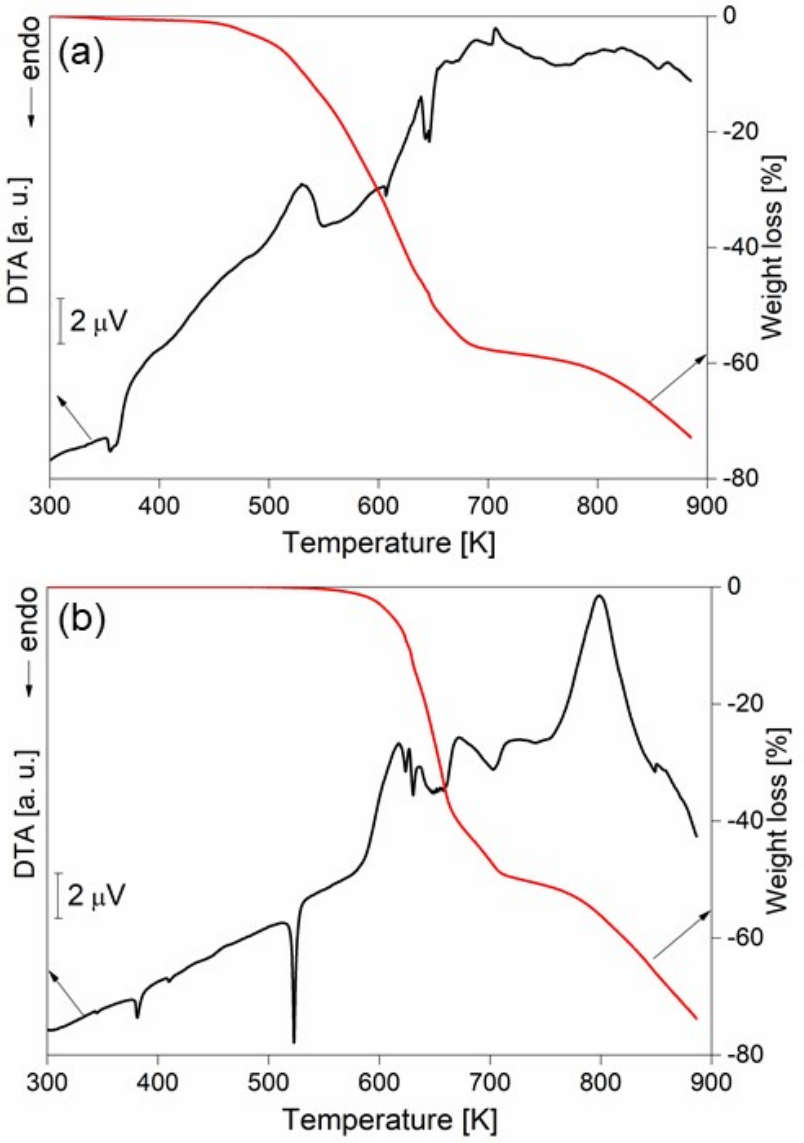

Figure S2. The results of the simultaneous TGA/DSC analyses for (a) **PCC** (sample mass m = 14.2541 mg 2 K·min^{-1}); (b) **PCB** (sample mass m = 13.7640 mg, 2 K·min^{-1})

3. Crystal structure analysis

Table S2. Experimental data for **PCC** and **PCB**.

Crystal data				
Empirical formula	$C_8H_{20}N_2CoCl_4$		$C_8H_{20}N_2CoBr_4$	
Formula weight (g mol^{-1})	344.99	344.99	522.83	522.83
Crystal system	Monoclinic	Orthorhombic	Monoclinic	Orthorhombic
Space group	$P2_1/c$	$Pna2_1$	$P2_1/n$	$Pna2_1$
Temperature (K)	290	350	295	400
Unit cell dimensions				
a (Å)	32.874 (8)	11.643 (5)	8.781 (3)	11.999 (5)
b (Å)	8.885 (3)	16.262 ()	11.383 (4)	16.686 (7)
c (Å)	21.428 (5)	8.420 ()	16.979 (5)	8.728 (4)
β (°)	90.02 (3)	90	93.71 (3)	90
V (Å^3)	6259 (3)	1594.2 (12)	1693.6 (10)	1747.5 (13)
Z	16	4	4	4
$D_{calc.}$ (g cm^{-3})	1.464	1.437	2.050	1.987
μ [mm^{-1}]	1.76	1.72	10.43	10.11
F(000)	2832	708	996	996
Crystal size	0.21×0.14×0.12	0.49×0.16×0.13	0.29×0.19×0.13	0.35×0.14×0.11
Data collection and Refinement				
Diffractometer	Xcalibur with Atlas CCD camera			
Monochromator	Graphite MoKα			
Radiation type, wavelength λ (Å)	MoKα, 0.71073	MoKα, 0.71073	MoKα, 0.71073	MoKα, 0.71073
Absorption correction	Analytical *CrysAlis PRO* 1.171.38.34a (Rigaku Oxford Diffraction, 2015) Analytical numeric absorption correction using a multifaceted crystal model based on expressions derived by R.C. Clark & J.S. Reid. (Clark, R. C. & Reid, J. S. (1995). Acta Cryst. A51, 887-897) Empirical absorption correction using spherical harmonics, implemented in SCALE3 ABSPACK scaling algorithm.			
Reflections collected/independent/ observed [R(int)]	68870/155515/6666 0.059	7562/3537/824 0.036	11375/3971/1890 0.035	16707/4107/772 0.077
Parameters	542	136	136	136
Goodness-of-fit on F^2	0.97	0.95	1.02	0.81
$R[F^2 > 2\sigma(F^2)]$, $wR(F^2)$	0.055, 0.142	0.093, 0.426	0.056, 0.143	0.081, 0.299
$\Delta\rho_{max}$, $\Delta\rho_{min}$ (e Å^{-3})	0.46, −0.40	0.24, −0.36	1.01, −0.99	0.31, −0.34
CCDC	2082868	2082869	2082870	2082871

Computer programs: *CrysAlis PRO* 1.171.38.34a (Rigaku OD, 2015), *CrysAlis PRO* 1.171.38.46 (Rigaku OD, 2015), *SHELXS* (Sheldrick, 2008), ShelXT (Sheldrick, 2015), *SHELXL* (Sheldrick, 2015), Olex2 (Dolomanov *et al.*, 2009).

Table S3. Selected geometric parameters (Å, °) for **PCC** at 290 K.

Co1—Cl1	2.250 (2)	Co1B—Cl1B	2.255 (2)
Co1—Cl2	2.2602 (19)	Co1B—Cl2B	2.2704 (19)
Co1—Cl3	2.2856 (18)	Co1B—Cl3B	2.2815 (19)
Co1—Cl4	2.2672 (19)	Co1B—Cl4B	2.2641 (19)
Co1A—Cl1A	2.248 (2)	Co1C—Cl1C	2.2542 (19)
Co1A—Cl3A	2.2832 (18)	Co1C—Cl2C	2.2726 (19)
Co1A—Cl2A	2.254 (2)	Co1C—Cl4C	2.2654 (19)
Co1A—Cl4A	2.2651 (19)	Co1C—Cl3C	2.2805 (19)
Cl1—Co1—Cl2	114.14 (8)	Cl1B—Co1B—Cl2B	107.56 (8)
Cl1—Co1—Cl3	108.16 (8)	Cl1B—Co1B—Cl3B	109.04 (8)

Cl1—Co1—Cl4	108.26 (8)	Cl1B—Co1B—Cl4B	113.77 (8)
Cl2—Co1—Cl3	108.07 (8)	Cl2B—Co1B—Cl3B	104.51 (7)
Cl2—Co1—Cl4	112.27 (8)	Cl4B—Co1B—Cl2B	113.02 (9)
Cl4—Co1—Cl3	105.52 (8)	Cl4B—Co1B—Cl3B	108.48 (8)
Cl1A—Co1A—Cl3A	109.00 (8)	Cl1C—Co1C—Cl2C	107.19 (7)
Cl1A—Co1A—Cl2A	112.87 (8)	Cl1C—Co1C—Cl4C	112.96 (8)
Cl1A—Co1A—Cl4A	108.12 (8)	Cl1C—Co1C—Cl3C	109.23 (8)
Cl2A—Co1A—Cl3A	109.12 (8)	Cl2C—Co1C—Cl3C	104.11 (7)
Cl2A—Co1A—Cl4A	112.73 (9)	Cl4C—Co1C—Cl2C	113.51 (8)
Cl4A—Co1A—Cl3A	104.63 (7)	Cl4C—Co1C—Cl3C	109.40 (8)

Table S4. Hydrogen-bond geometry (Å, °) for **PCC** at 290 K.

D*—H···*A	***D*—H**	**H···*A***	***D*···*A***	***D*—H···*A***
N1—H1*A*···Cl1	0.89	2.85	3.394 (5)	121
N1—H1*A*···Cl3	0.89	2.53	3.309 (6)	146
N1—H1*B*···Cl2*C*^{i}	0.89	2.41	3.247 (6)	158
N6—H6*A*···Cl2	0.89	2.32	3.195 (7)	168
N6—H6*B*···Cl2*C*^{ii}	0.89	2.84	3.571 (8)	141
N6—H6*B*···Cl3*C*^{ii}	0.89	2.65	3.352 (6)	137
N1*A*—H1*AA*···Cl1*A*	0.89	2.83	3.342 (6)	118
N1*A*—H1*AA*···Cl3*A*	0.89	2.48	3.275 (7)	148
N1*A*—H1*AB*···Cl4*A*^{iii}	0.89	2.48	3.293 (7)	152
C4*A*—H4*AB*···Cl2*C*^{iv}	0.97	2.83	3.655 (11)	143
N6*A*—H6*AA*···Cl3*A*^{iv}	0.89	2.59	3.315 (6)	139
N6*A*—H6*AB*···Cl2*A*	0.89	2.29	3.175 (8)	173
N1*B*—H1*BA*···Cl1*B*	0.89	2.82	3.365 (5)	121
N1*B*—H1*BA*···Cl3*B*	0.89	2.56	3.314 (7)	144
N1*B*—H1*BB*···Cl2*B*^{v}	0.89	2.42	3.263 (6)	158
N6*B*—H6*BA*···Cl2*B*^{vi}	0.89	2.86	3.593 (8)	141
N6*B*—H6*BA*···Cl3*B*^{vi}	0.89	2.66	3.377 (7)	138
N6*B*—H6*BB*···Cl4*B*	0.89	2.33	3.197 (8)	165
C10*B*—H10*F*···Cl3*B*	0.97	2.92	3.795 (11)	150
N1*C*—H1*CA*···Cl1*C*	0.89	2.83	3.369 (5)	121
N1*C*—H1*CA*···Cl3*C*	0.89	2.53	3.306 (7)	146
N1*C*—H1*CB*···Cl4^{vii}	0.89	2.47	3.285 (7)	152
C4*C*—H4*CB*···Cl2*B*	0.97	2.72	3.597 (11)	151
N6*C*—H6*CA*···Cl4*C*	0.89	2.30	3.165 (7)	164
N6*C*—H6*CB*···Cl3^{viii}	0.89	2.47	3.280 (6)	152

Symmetry codes: (i) *x*, *y*−1, *z*; (ii) *x*, −*y*+3/2, *z*+1/2; (iii) −*x*+1, −*y*+2, −*z*+1; (iv) −*x*+1, *y*−1/2, −*z*+1/2; (v) −*x*+2, −*y*+1, −*z*; (vi) −*x*+2, *y*−1/2, −*z*+1/2; (vii) *x*, *y*+1, *z*; (viii) *x*, −*y*+1/2, *z*−1/2.

Table S5. Selected geometric parameters (Å, °) for **PCC** at 350 K.

Co1—Cl3	2.240 (6)	Co1—Cl2	2.194 (18)
Co1—Cl1	2.255 (6)	Co1—Cl4	2.287 (16)
Cl3—Co1—Cl1	108.6 (3)	Cl2—Co1—Cl3	106.6 (8)
Cl3—Co1—Cl4	111.5 (9)	Cl2—Co1—Cl1	112.7 (6)
Cl1—Co1—Cl4	105.2 (6)	Cl2—Co1—Cl4	112.1 (5)

Table S6. Hydrogen-bond geometry (Å, °) for **PCC** at 350 K.

D*—H···*A	***D*—H**	**H···*A***	***D*···*A***	***D*—H···*A***
N1—H1*B*···Cl1	0.89	2.78	3.43 (3)	131
C2—H2*A*···Cl4^{i}	0.97	2.79	3.57 (4)	137
C9—H9*B*···Cl3^{ii}	0.97	2.74	3.60 (6)	149
C10—H10*A*···Cl4^{iii}	0.97	2.74	3.66 (6)	158
N6—H6*B*···Cl2	0.89	2.70	3.44 (4)	141

Symmetry codes: (i) −*x*+1, −*y*+1, *z*−1/2; (ii) −*x*, −*y*+1, *z*+1/2; (iii) −*x*, −*y*+1, *z*−1/2.

Table S7. Selected geometric parameters (Å, °) for **PCB** at 295 K.

Br1—Co1	2.3921 (16)	Co1—Br2	2.4001 (15)
Br4—Co1	2.3867 (15)	Co1—Br3	2.3963 (16)
Br1—Co1—Br2	109.00 (5)	Br4—Co1—Br2	109.95 (6)
Br1—Co1—Br3	110.99 (6)	Br4—Co1—Br3	109.10 (6)
Br4—Co1—Br1	111.79 (5)	Br3—Co1—Br2	105.84 (6)

Table S8. Hydrogen-bond geometry (Å, °) for **PCB** at 295 K.

D*—H···*A	***D*—H**	**H···*A***	***D*···*A***	***D*—H···*A***
N1—H1*A*···Br2^{i}	0.89	2.72	3.538 (8)	153
N1—H1*B*···Br1	0.89	2.82	3.423 (6)	127
N1—H1*B*···Br3	0.89	2.93	3.672 (8)	142
N6—H6*A*···Br3^{ii}	0.89	2.76	3.583 (11)	154
N6—H6*B*···Br4	0.89	2.80	3.510 (11)	138
C10—H10*A*···Br2^{ii}	0.97	2.79	3.700 (14)	157
C10—H10*B*···Br4	0.97	2.95	3.663 (18)	131
C9—H9*A*···Br3^{iii}	0.97	2.99	3.950 (18)	173
C9—H9*B*···Br1^{iv}	0.97	3.09	3.89 (2)	141

Symmetry codes: (i) −*x*, −*y*+1, −*z*+1; (ii) −*x*, −*y*, −*z*+1; (iii) −*x*+1, −*y*, −*z*+1; (iv) *x*, *y*−1, *z*.

Table S9. Selected geometric parameters (Å, °) for **PCB** at 400 K.

Co1—Br1	2.374 (4)	Co1—Br2	2.384 (12)
Co1—Br3	2.386 (4)	Co1—Br4	2.334 (12)
Br1—Co1—Br3	110.60 (16)	Br4—Co1—Br1	110.1 (4)
Br1—Co1—Br2	109.1 (4)	Br4—Co1—Br3	110.2 (4)
Br2—Co1—Br3	105.6 (4)	Br4—Co1—Br2	111.1 (2)

Table S10. Hydrogen-bond geometry (Å, °) for **PCB** at 400 K.

D*—H···*A	***D*—H**	**H···*A***	***D*···*A***	***D*—H···*A***
N1—H1*B*···Br1	0.89	3.08	3.69 (4)	128
C2—H2*A*···Br4^{i}	0.97	3.05	3.72 (5)	127
N6—H6*B*···Br2	0.89	2.80	3.52 (3)	139
C9—H9*B*···Br3^{ii}	0.97	3.25	3.95 (9)	131

Symmetry codes: (i) −*x*+1, −*y*+1, *z*−1/2; (ii) −*x*, −*y*+1, *z*+1/2.

4. Optical properties

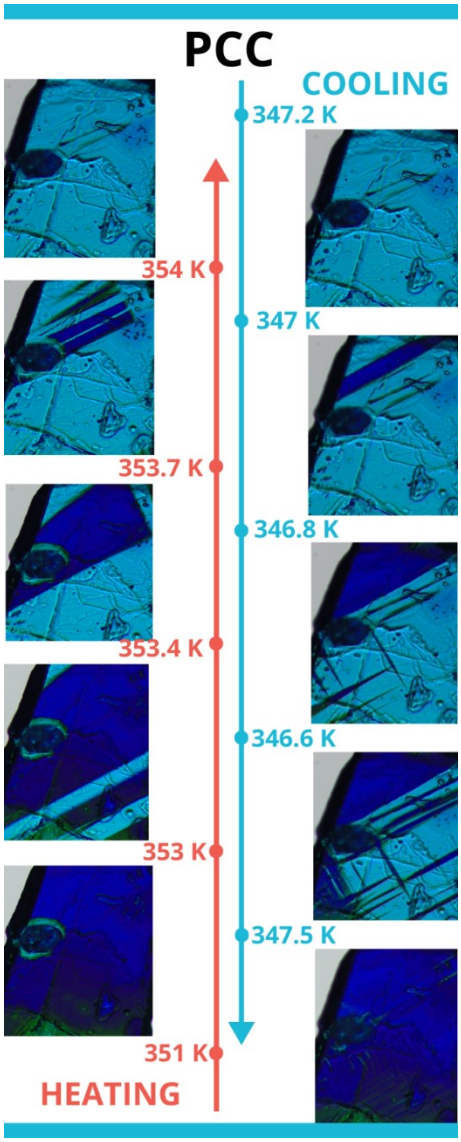

Figure S13. Evolution of domain structure of **PCC**. The figure contains an approximate temperatures.

Between RT and 353 K the **PCC** sample is monodomain, then at approx. 353.4 K the domain walls appear. In Phase I (above 354 K), the sample becomes mono-domain. This means that the Phase I can be considered as prototypical/paraelastic one. During the cooling process, below 347 the evolution of the phase front and appearing of the ferroelastic domain structure is well visible. The appearance of the domain structure only in the close vicinity of PT (I→II) proves that strong distortion of the crystal lattice initiates the formation of domains. Below 347.5 K the ferroelastic domains disappeared in spite of the fact that over the all Phase (II) the compound is ferroelastic.

5. Proton Magnetic Resonance (second moment (M_2)).

The temperature dependence of the second moment of the proton resonance lines, M_2, of **PCB** and **PCC** are shown in Figure S3. For **PCB** the second moment values decrease from about 41 G^2 at 107K to below 3 G^2 at 385 K. Also for **PCC** is observed the narrowing of ^1H NMR line from about 54 G^2 at 107 K to plateau below 4 G^2 at 380 K. These both high values of the second moment at the lowest temperatures confirms the influence of the present of the paramagnetic $^{59}Co(II)$ in crystal structure of both studied compounds. This fact denotes not only the presence of the ^1H-^{59}Co interaction next to the ^1H-^1H interaction[1] but the strongly quadrupolar nature additionally disturb the ^1H-^{59}Co couplings increasing the width of measured NMR line.[2]

Table S11 Activation energies, correlation times and motional constants evaluated for **PCB** and **PCC**.

Compound	**PCB**	**PCC**
E_{a1} [kJ/mol]	4.45	4.45
τ_{01} [s]	$3.75\ 10^{-10}$	$3.75\ 10^{-10}$
K_1 [Hz^2]	$1.75\ 10^{11}$	$4.76\ 10^{11}$
E_{a2} [kJ/mol]	3.35	3.35
τ_{02} [s]	$3.8\ 10^{-11}$	$3.8\ 10^{-11}$
K_2 [Hz^2]	$1.26\ 10^{12}$	$1.26\ 10^{12}$

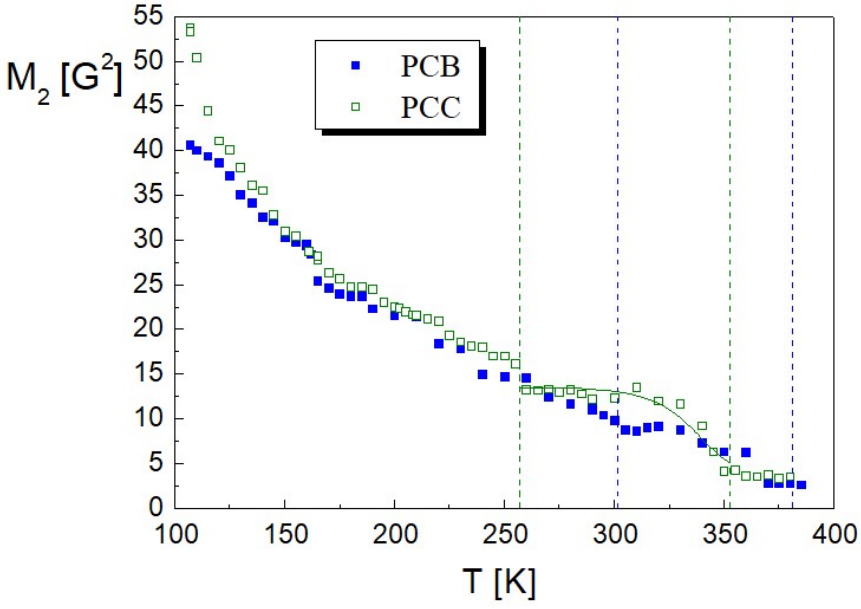

Figure S12. Temperature dependence of ^1H NMR second moment of **PCB** and **PCC**.

The calculations of M_2 based on the crystal structures of compounds containing the pyrrolidinium cations gave the values *ca.* 18-20 G^2 in the rigid state. In Figure S3 the second moment drops to such values only above 200 K where the domination of quadrupolar interaction gradually vanishes. At PT temperatures there are visible a distinct change in slopes or sudden drop of the M_2 values. In the case of **PCC** around 257 PT **PCC** a of small drop *ca*. 3 G^2 is visible. In turn above 353 K the plateau begins without any drop in M_2 values. It is the opposite for **PCB**. In case of **PCC** the reduction of M_2 from 13 G^2 to 4 G^2 in temperature range 257 K – 353 K has been fitted with standard BBP formula and the calculated theoretical solid line is drawn in Figure S12. For the chosen reduction of second moment the found activation energy is to be 54.9 $kJ \cdot mol^{-1}$ with the correlation time of 4.36 10^{-14} s. Considering the result of this numerically analyzed reduction of the second moment of ^1H NMR line it may be concluded that the pyrrolidinium cation in this temperature range is probably performing packing motion of the pyrrolidinium cation between the twisted and envelope conformations or rotations about the pseudo-C5 axis. At the highest temperatures (above 350-360 K) the isotropic rotations and cationic self-diffusion are expected taking into account the previous results for compounds containing in the structure pyrrolidinium.[3-6]

References:

1 A. Abragam, The Principles of Nuclear Magnetism. Oxford University Press, Oxford, 1961.
2 J. D. Epperson, Li-June Ming, B. D. Woosley, G. R. Baker, and G. R. Newkome, *Inorg. Chem*., 1999, **38**, 4498-4502.
3 C. P. Slichter, Principles of Magnetic Resonance, Springer Ser. Solid-State Sci., Berlin, 1990.
4 D. Kruk, Theory of Evolution and Relaxation of Multi-Spin Systems: Application to Nuclear Magnetic Resonance (NMR) and Electron Spin Resonance (ESR), Arima Publishing, UK, 2007.
5 J. Kowalewski, D. Kruk and G. Parigi, *Adv. Inorg. Chem*., 2005, **57**, 41-104.
6 D. Kruk and J. Kowalewski, *Mol. Phys*., 2003, **101**, 2861-2874.

6. HF EPR spectroscopy

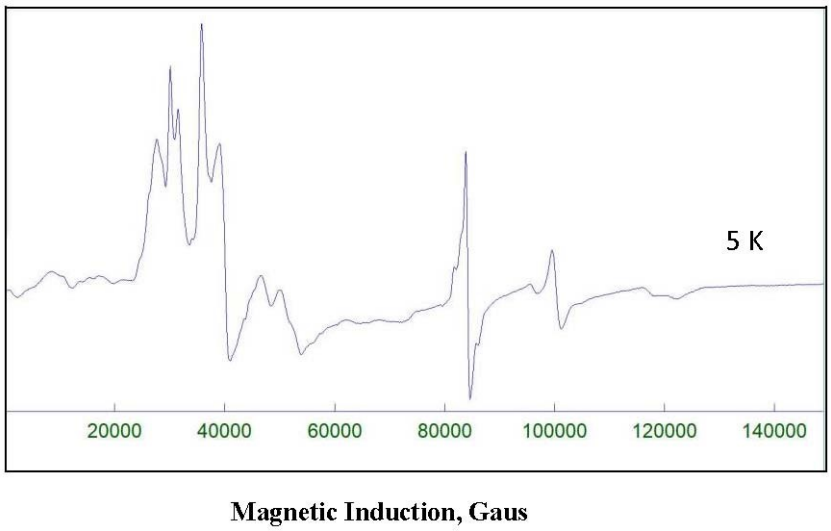

Figure S14. High-field EPR spectra of **PCC** recorded at 5 K.

7. Magnetic properties

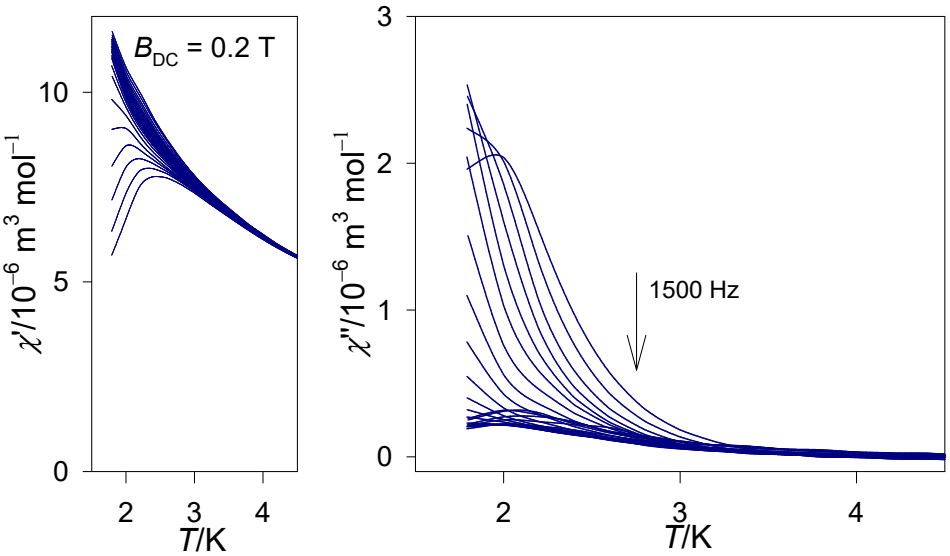

Figure S15. Temperature evolution of the AC susceptibility components for **PCC** at B_{DC} = 0.2 T.

Table S12. Temperature dependence of AC susceptibility parameters for **PCC** at B_{DC} = 0.2 T [a]

T/K	$R(\chi')$ /%	$R(\chi'')$ /%	χ_S	χ_{LF}	α_{LF}	τ_{LF} / s	χ_{HF}	α_{HF}	τ_{HF} /10^{-6} s	x_{LF}	x_{HF}
1.8	0.51	3.2	4.37(8)	5.6(9)	.49(17)	3.4	12.4(8)	.17(1)	342(7)	.16	.84
2.0	0.16	1.5	3.94(8)	5.5(3)	.54(4)	2.3	11.5(2)	.24(1)	129(3)	.21	.79
2.2	0.36	3.6	3.9(5)	5.6(9)	.60(8)	2.4	10.9(5)	.30(3)	50(9)	.25	.75
2.4	0.39	6.7	4.5(11)	5.9(16)	.60(12)	2.2	10.1(5)	.35(6)	25(15)	.26	.74
2.6	0.31	9.1	4.8(23)	5.9(28)	.60(15)	3.7	9.5(6)	.44(10)	10	.26	.74
2.8	0.23	9.9	4.8	5.7	.60	2.5	8.7(4)	.49(15)	3.2	.22	.78

[a] χ_S – adiabatic susceptibility, χ_i – isothermal susceptibility, α_i – distribution parameter, τ_i – relaxation time, x_i – mole fraction for the i-th relaxation channel (LF or HF); $R(\chi')$ and $R(\chi'')$ – discrepancy factors of the fit. Standard deviations of the varied parameters in parentheses.